International Journal of Mechanical Sciences 238 (2023) 107830

Contents lists available at ScienceDirect

International Journal of Mechanical Sciences

journal homepage: www.elsevier.com/locate/ijmecsci

Anisotropic metal foam design for improved latent heat thermal energy storage in a tilted enclosure

Mehdi Ghalambaz [a], Mutabe Aljaghtham [b], Ali J. Chamkha [c], Abdelkader Abdullah [b,d], Abdullah Alshehri [b], Mohammad Ghalambaz [e,*]

[a] Institute of Research and Development, Duy Tan University, Da Nang 550000, Vietnam
[b] Department of Mechanical Engineering, College of Engineering in Al-Kharj, Prince Sattam Bin Abdulaziz University, Al-Kharj 11942, Saudi Arabia
[c] Faculty of Engineering, Kuwait College of Science and Technology, Doha District, Kuwait
[d] Mechanical Power Engineering Department, Faculty of Engineering, Tanta University, Tanta 31521, Egypt
[e] Department of Theoretical Mechanics, Tomsk State University, 36 Lenin Ave., Tomsk 634050, Russia

ARTICLE INFO

Keywords:
Anisotropic metal foam
Anisotropic angle
Solid-liquid phase transition
Latent heat thermal energy storage
Inclination angle

ABSTRACT

The metal foams are a promising candidate for the enhancement of heat transfer in latent heat thermal energy storage (LHTES) units. These foams can be synthesized with engineered local properties such as improved thermal conductivity or permeability in a specified direction. However, the impact of using anisotropic metal foams for thermal energy storage has not been addressed yet. In the current research, an anisotropic metal foam was modeled mathematically with engineered local properties in perpendicular directions. The solid-liquid phase transition of the copper-coconut oil LHTES unit was simulated using the finite element method. The anisotropic metal foam was defined by using an anisotropic parameter and angle. The simultaneous impact of the mounting tilt angle and the anisotropic angle of the copper foam were addressed in the phase transition behavior and charging time of the LHTES unit. The results revealed that the anisotropic angle could notably impact the thermal energy storage power. An optimum tilt angle of -45° or +45° along with a 0° anisotropic angle could lead to the maximum charging power. Thus, designing an LHTES unit using an anisotropic metal foam could save the charging about 15% (for a -45° inclination angle) and 20% (for zero inclination angle) compared to a regular metal foam. Such save in the charging time is without any penalty on the weight increase or capacity reduction for the LHTES unit.

1. Introduction

The increasing energy consumption has caused the global energy crisis and environmental damage. It draws attention to renewable energy sources; nevertheless, because of their intermittent and fluctuating nature, notably solar energy, attempts have been made to address the limitations and enhance TES (thermal energy storage) systems' energy efficiency have increased [1]. TES systems can be classified as chemical, sensible, and latent heat (LHS) [2]. Several advantages of LHS have drawn considerable attention, including high thermal energy storage density, system resiliency, low costs, and generally consistent temperatures for charging and discharging [3]. On the other hand, long-term TES requires particular materials, sophisticated methods, and complex installations. Specific applications need materials with high thermal capacity and a low melting point; these materials, often referred to as PCMs (phase change materials), now provide broadly responsive options to a wide range of applications. The essence of their concept is the PCM charge (melting)/discharge (solidification) heat energy via latent heat phenomenon during the phase change process. PCM's poor heat conduction capability limits charging and discharge operations and fast heat transmission. Different approaches, such as heat pipes [4], fins and extended surfaces [5–7], carbon nanotubes [8], and MF (metal foam) [9], have been developed to overcome the mentioned limitation.

For example, Najim et al. [10] employed fins with different cross sections to reduce the melting time in a triple tube shell-tube thermal energy storage unit. The results showed the cross-section shape of the fins could influence the melting time by about 8%. Tiji et al. [11] used frustum tubes in shell-tube thermal storage and showed using the frustum tubes can reduce the melting time by 25.6%. Using multiple PCMs [12] or wavy-elliptical shape tubes [13] could also reduce the

* Corresponding author.
E-mail addresses: mehdighalambaz@duytan.edu.vn (M. Ghalambaz), a.chamkha@kcst.edu.kw (A.J. Chamkha), m.ghalambaz@gmail.com (M. Ghalambaz).

https://doi.org/10.1016/j.ijmecsci.2022.107830
Received 12 August 2022; Received in revised form 2 October 2022; Accepted 8 October 2022
Available online 9 October 2022

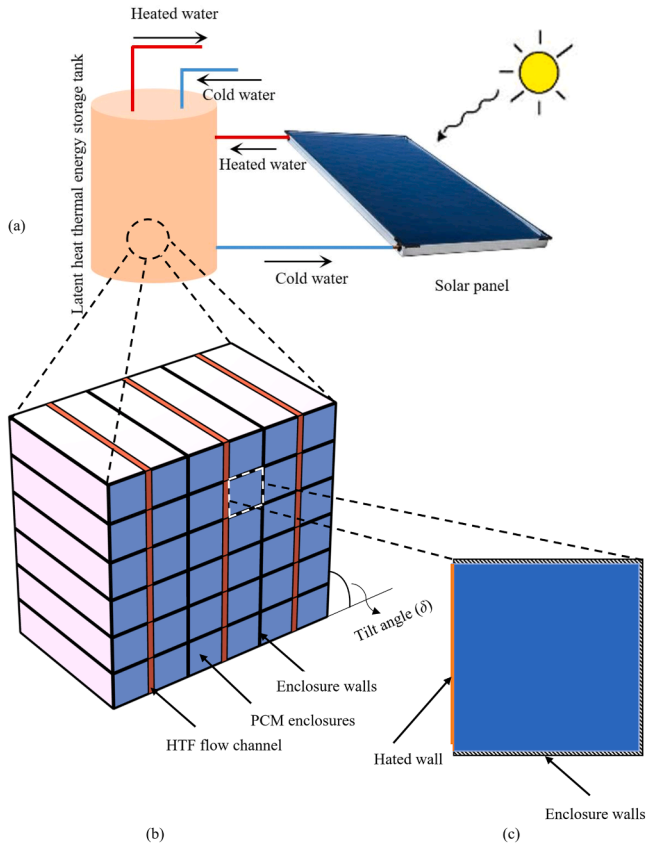

Fig. 1. A schematic view of an LTHES unit and its modeling approach. A solar collector absorbs the heat and transfers it to an LHTES, where the PCM modules store the heat through a melting process. Each of the storage modules can be considered a rectangular channel which was modeled as a 2D rectangle.

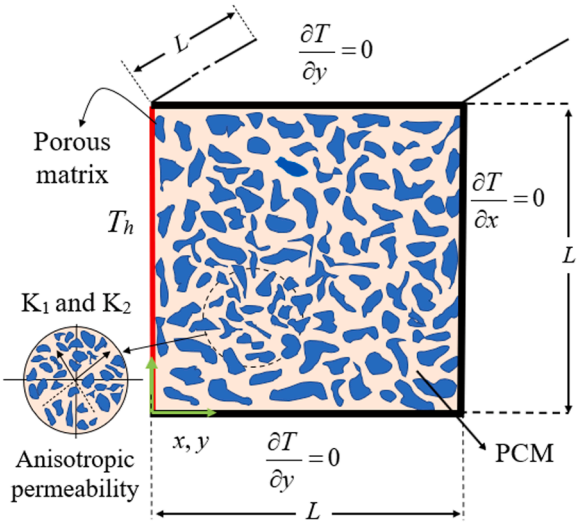

Fig. 2. A detailed diagram of the LHTES unit's physical model and the boundary conditions. The vertical wall is subject to a forced convection flow of working fluid from the solar collector and is considered an isothermal hot surface. The rest of the walls are insulated. The anisotropic porous medium can be placed at an angle γ with respect to the horizon.

melting time.

Previous investigations demonstrated that MF promotes melting and the solidification process in latent heat thermal energy storage (LHTES) units. Dede and Joshi [14] developed MFPCM batteries that run at lower

Table 1
Thermophysical properties of the Coconut oil and the nano additives [53,54].

Properties	Copper foam	Coconut oil Solid* (15 °C)	Liquid (32 °C)
ρ (kg/m^3)	8900	920	914 ± 0.11%
μ (Ns/m^2)	–	–	0.0326 ± 3%
k (W/m K)	380	0.228	0.166 ± 1.2%
C_p (J/kg K)	386	3750	2010 ± 0.2%

* The fusion temperature was 24 °C and $L_f = 103$ kJ/kg.

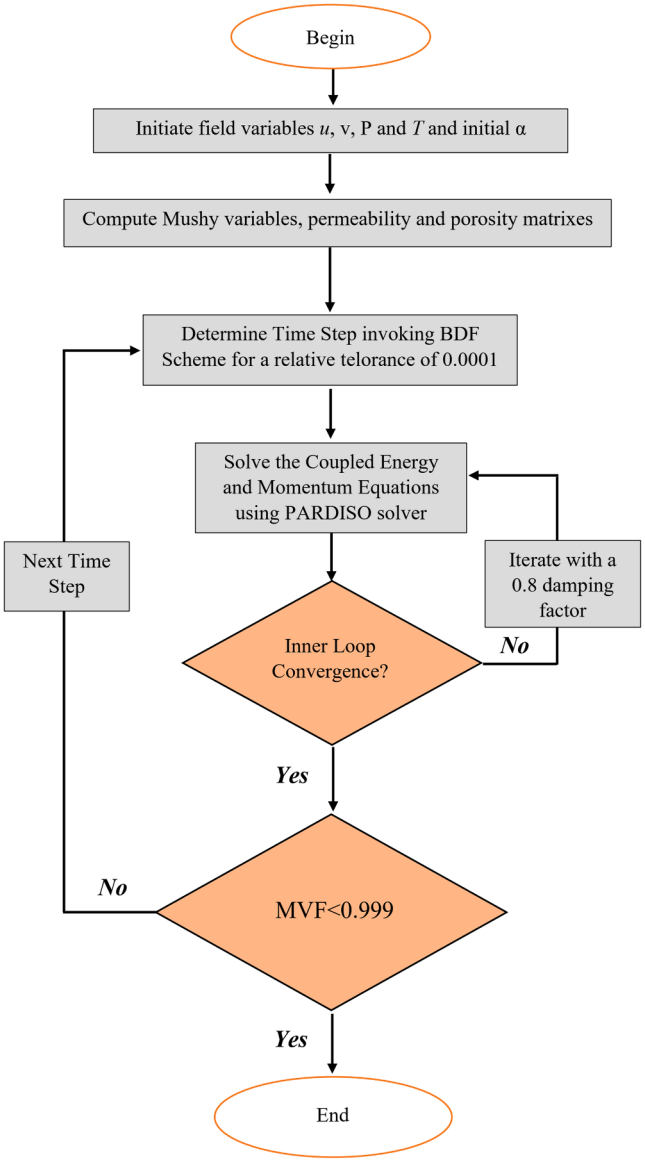

Fig. 3. Flowchart of the numerical computations. The code starts with initial conditions and then computes the variable properties. The governing equations are computed in a coupled approach. The computations were ended when the full melting (MVF ~ 0.999) reached.

temperatures and provide more power; this unique battery technology can produce more energy while also prolonging the battery's lifespan. Ferfera et al. [15] investigated the porosity of porous composites and discovered that higher porosity leads to enhanced thermal conductivities, while small pores lead to homogeneous melting fronts inside the composite.

Heat transfer in MFs is influenced by anisotropy [16]. Gravity,

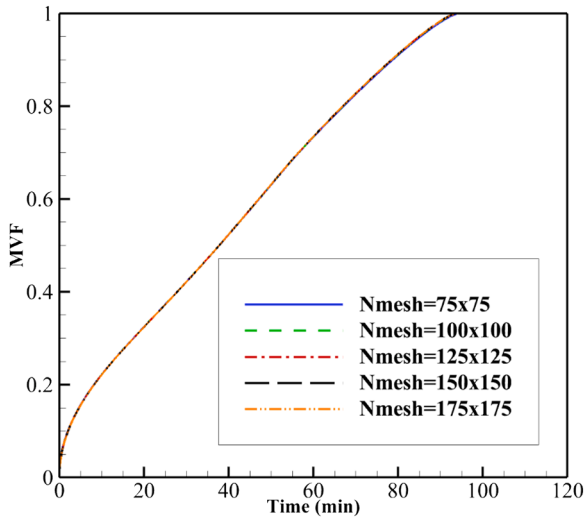

Fig. 4. Influence of mesh resolution on liquid fraction when $\delta = 45°$, $\gamma = 45°$, and K_n=0.3. The MVF curves are very close to each other. Thus, it can be concluded that the utilized mesh size along with automatic time step control can solve the model with good accuracy. A mesh size of 100 × 100 is adopted for the computations.

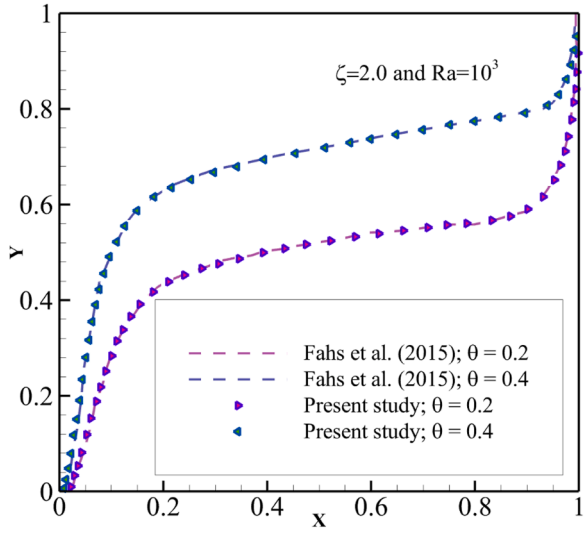

Fig. 5. A comparison between the isotherms of [66] and current computations. The results for temperature curves show excellent agreement with the literature studies for natural convection in an anisotropic porous medium.

compression, and viscous stresses generate conductivity anisotropy in MFs embedding with PCM [17]. Therefore, the structural properties of the porous medium are critical to the composite PCM unit's phase change and heat transfer capabilities [18]. Yang et al. [19] investigated the melting properties of porosity gradient MFPCM numerically. They discovered that MF porosity increasing from bottom to top improved the melting rate. Zhu et al. [20] examined the effects of porosity grade and fin thickness by incorporating a fin into an MFPCM with graded porosity. According to research, the presence of fins altered the melting sequence, whereas graded foams enhanced the rate of heat transfer. Using multi-segment MFs of varying porosity revealed that cascaded foams produced more stable temperatures, decreasing phase change speed [21]. Xu et al. [22] conducted a computational study to determine the optimal values for several foam layers. Three samples of copper foam were analyzed to strike a balance between material cost and phase change rate. Joshi and Rathod [23] investigated the effect of optimal MF placement and concluded that MF positioned at higher temperature gradients may improve heat transfer. Consequently, a properly calibrated MF could mitigate its detrimental impact on heat convection while simultaneously reducing the TES's additional expenses. Moreover, a study performed by Guo et al. [24] showed mounting MF under contractual pressure can save the phase change time about 13.9%.

Liu et al. [25] showed using several layers of MF with different porosities and creating a porosity gradient can influence the charging time. An aiding configuration of MF layers can reduce the charging time by 17.9%. Vijay et al. [26] found that the inlet flow direction influenced the heat transfer rates associated with foam due to its anisotropy. Yang et al. [27] conducted a numerical study investigating MFs with non-uniform porosity by optimizing pore density and average porosity. A reduction in melting rate is caused by decreasing the porosity from the bottom to the top due to enhanced natural convection. In an experiment and a numerical study, Huang et al. [28] demonstrated that the melting rate of the PCM increased as the porosity of the MF decreased. Bamdezh et al. [29] developed a TES and studied the effect of MF anisotropy on the system's performance. Findings indicated that increasing the tangential conductance increases the melting rate and average cell temperature; Also, rising axial heat conductivity has a good impact on reducing cell temperature differentials. Yu et al. [30] studied the anisotropic properties of two kinds of pore geometries. There is evidence that when using MFs, it is essential to consider their anisotropic properties. The anisotropic thermal conduction of an MFPCM composite was explored by Ren et al. [31], which enhanced the thermal efficiency of a TES unit more than isotropic porous media. Their findings showed significant improvement in performance and cost savings if anisotropic woven MF was designed in the desired direction. Several works of literature [32, 33] have also reached similarly definitive conclusions.

Obtaining the best storage design, both in terms of capacity and charging/discharging times, requires a thorough understanding of the thermodynamics of PCM cavities during their development. The role that natural convection plays in influencing phase transitions in the liquid phase of the storage material is one of the major concerns. Natural convection is affected by geometric considerations (such as cavity orientation) and PCM properties. The MF reduces natural convection, according to experimental studies employing different inclination degrees of the TES [34]. A cavity's inclination angle substantially affects phase change efficiency since it may drastically alter natural convection flow governed by buoyancy [35]. Dhaidan and Khodadadi [36] discussed natural convection melting in various geometries. The increase in heat transfer due to natural convection increases with enclosure size, according to Vogel et al. [37]. Iasiello et al. [38] discovered that the thermal conductivity of MFs with varying porosities is related to cell elongation [39]; Also, they tested aluminum foams combined with PCM under various MF characteristics (porosity, temperature, pore sizes (PPIs), orientation) [40]. Porosity reduction significantly reduced melting time, whereas PPI and orientation have little effect. Xie et al. [41,42] evaluated the impact of MF structure, volume percentage, and orientation on a new design.

Yazici et al. [43] studied the effects of fin number and angle of inclination on the thermal performance of a PCM cavity heated from its broadside. As a result of their results, the inclination angle and the number of fins significantly impact the creation of convective cells in the liquid PCM domain, thereby influencing heat transfer and operational time. A study conducted by Kamkari and Groulx [44] examined the impact of the orientation on phase change rate in rectangular enclosures with 1-fin and 3-fin fins, finding that even little inclinations promote melting. Karami and Kamkari [45] confirmed this by statistically examining this type of finned cavity with inclination angles ranging from 0 to 180 degrees.

Samimi Behbahan et al. [46] numerically investigated the role of MF porosity as well as shell aspect ratio on PCM melting in an LHTES unit. Meng et al. [47] quantitatively investigated the effect of inclination angle on the thermal behavior of PCM in a hollow filled with copper

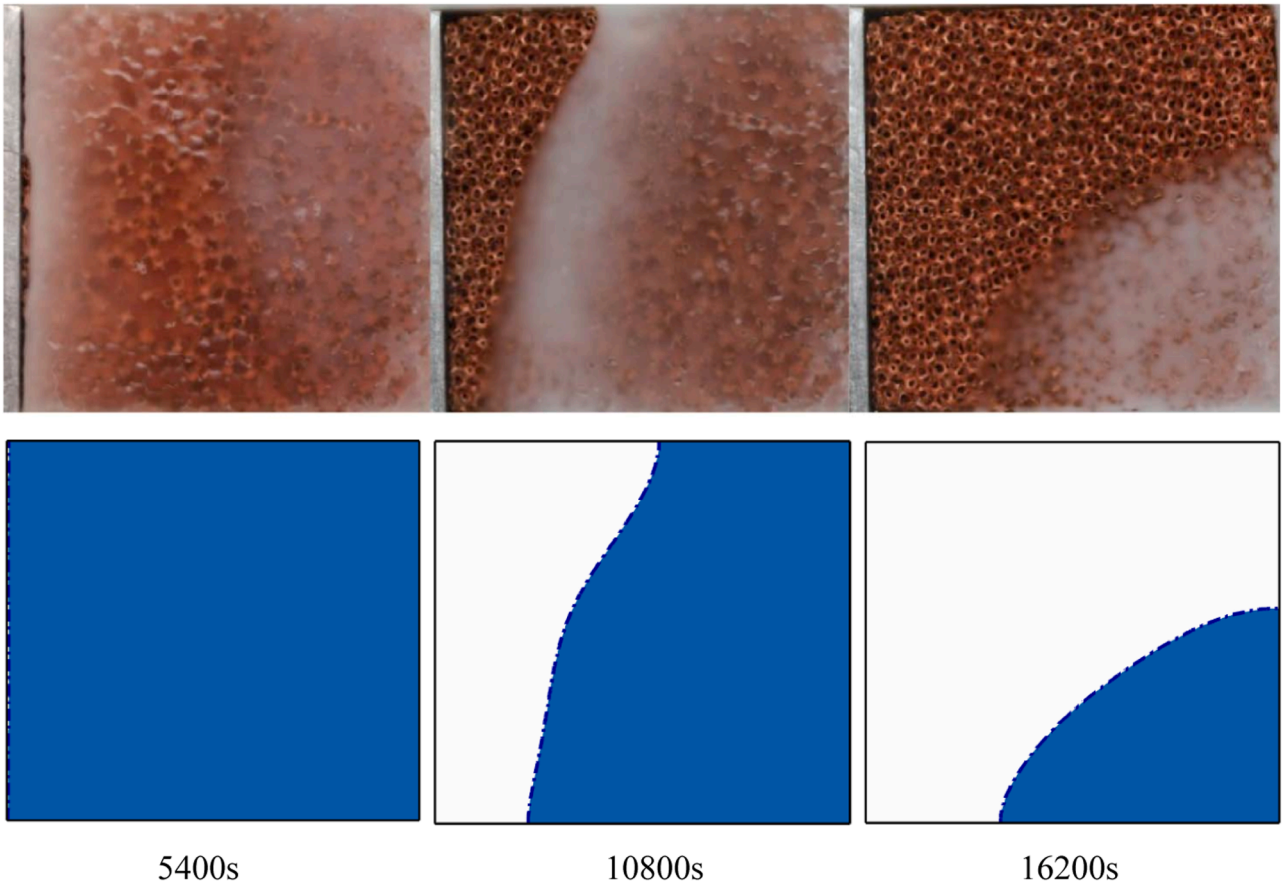

Fig. 6. The empirical [67] and theoretical melting fronts for phase transition of uniform composite copper foam – paraffin. The comparison between the observed (experimental images) melting front and the simulation results show good agreement for melting PCM in metal foams.

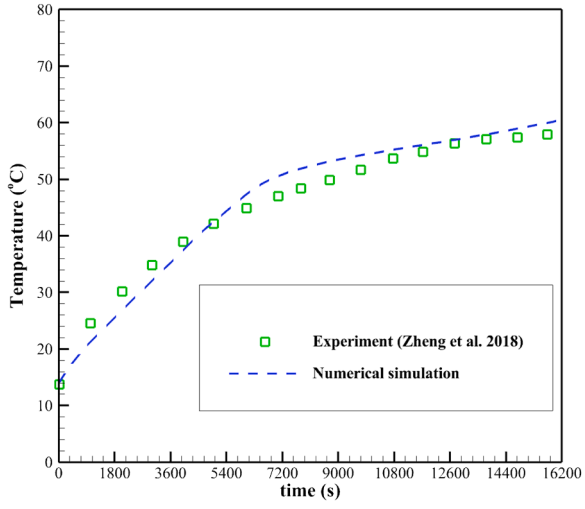

Fig. 7. A comparison between the empirical [67] measurements and simulated temperature in the present study. A good agreement between the present simulation and literature experiment can be observed.

foam fins. The results demonstrated that the inclination angle significantly impacted PCM thermal performance. Bouzennada et al. [48] studied the thermal behavior of a PCM filling a rectangular capsule with and without including a mid-separating fin with varied inclination angles.

Tian et al. [49] investigated the influence of enclosure inclination on

Table 2
The simulated cases and corresponding total stored energy (ES), charging time, and charging power when MVF = 0.99.

Cases	γ (deg)	δ (deg)	ES (kJ)	Charging time (min)	Charging power (W)
C1	-90	-45	283.0	105.9	44.5
C2	-90	-22.5	281.0	115.4	40.6
C3	-90	0	274.6	167.5	27.3
C4	-90	22.5	281.1	115.4	40.6
C5	-90	45	283.0	105.9	44.5
C6	-45	-45	288.9	91.3	52.7
C7	-45	-22.5	287.1	94.5	50.6
C8	-45	0	285.0	110.2	43.1
C9	-45	22.5	285.3	89.4	53.2
C10	-45	45	287.3	81.1	59.0
C11	0	-45	292.7	71.4	68.4
C12	0	-22.5	291.5	74.5	65.2
C13	0	0	277.4	97.1	47.6
C14	0	22.5	291.5	74.5	65.2
C15	0	45	292.7	71.3	68.4
C16	45	-45	287.3	81.1	59.0
C17	45	-22.5	285.3	89.4	53.2
C18	45	0	284.9	110.2	43.1
C19	45	22.5	287.1	94.5	50.6
C20	45	45	288.9	91.3	52.7
C21	90	-45	283.0	105.9	44.5
C22	90	-22.5	281.1	115.4	40.6
C23	90	0	281.1	115.4	40.6
C24	90	22.5	281.1	115.4	40.6
C25	90	45	283.0	105.9	44.6

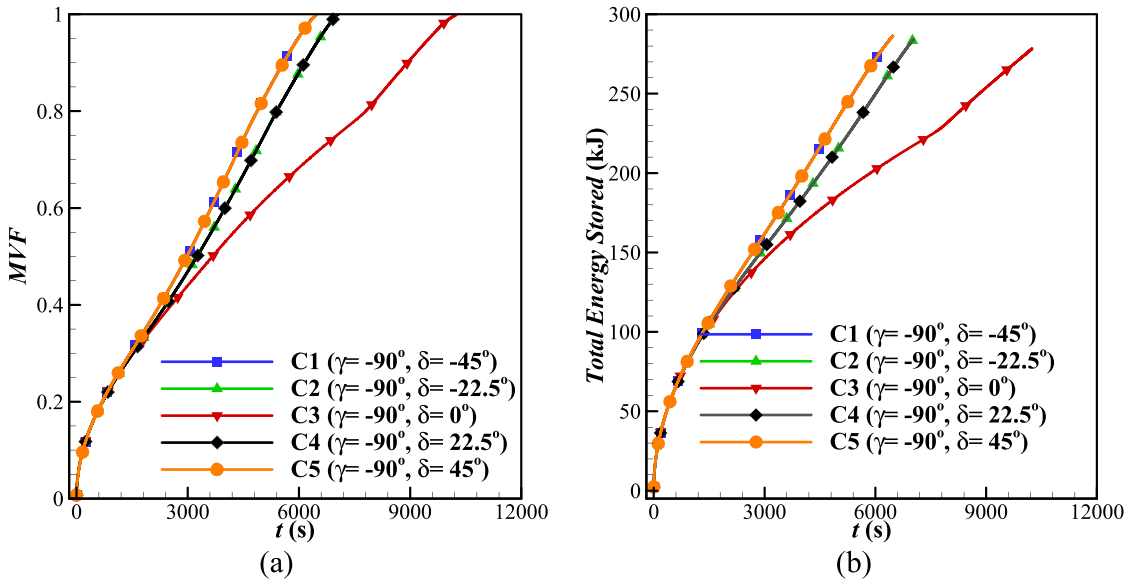

Fig. 8. Effect of inclination angle on; (a) Melting volume fraction and (b) Total energy stored in the anisotropic porous medium with $\gamma = -90^{\circ}$ (Cases C1–C5). Cases $\delta = +45^{\circ}$ and -45° provide the shortest melting time and the highest rate of thermal energy storage. Case $\delta = 0^{\circ}$ corresponds to the longest melting time and lowest rate of thermal energy storage.

melting behaviors using computational models with tilted settings. According to the results, independent of inclination angles, the time needed for complete melting of metal foam increased significantly with porosity. The variation in pore density had less of an effect on the total melting time. Kasper et al. [50] examined the impact of various aluminum proportions and fin spacings on charging/discharging speeds in different PCM cavity orientations. Angle significantly affects the thermophysical melting behavior, while natural convection has little effect on solidification. Li et al. [51] calculated the heat storage capacity of seven graded MFPCM composite models with 0, 30, 60, 90, 120, 150, and 180 degrees inclinations. Under the impact of changing inclination angles, Lu et al. [52] assessed the phase change rate of a TES with a rectangular encapsulation. Although the MF ligaments significantly reduced natural convection, heat behavior and melting capabilities varied with tilt degree.

A literature survey found that TES systems in phase transition need further attention. It is known that graded MF can accelerate PCM melting; however, there has not been much research on the melting behavior of graded MF composite PCM with anisotropic properties (varied orientations). The present work models anisotropic MF and addresses the influence of various orientations on the heat transfer performance of an inclined LHTES unit for the first time.

2. Model description and mathematical formulation

In this section, first, the physical model and the mathematical governing equations are introduced. Then, the corresponding boundary conditions are provided. Finally, the parameters of interest (the design parameters) are introduced mathematically.

2.1. Physical model

Fig. 1(a) shows a schematic view of a solar water heating system with a latent heat thermal energy storage unit. The excess solar heat can be stored in the LHTES unit and released later for heating applications on demand. A section of a pack of storage unit's internal design is depicted in Fig. 1(b), and a specific 2D view of a storage unit is plotted in Fig. 1(c). Fig. 2 illustrates a detailed view of Fig. 1(c), including the boundary conditions. The enclosure is a channel of size $L = 120$ mm filled with copper foam coconut oil and heated from a side wall. Copper foam is an anisotropic metal foam. The heated heat transfer fluid (HTF) leaves the solar collector at a hot temperature T_h and enters the LHTES, and it flows through the HTF flow channels from the front to the back of the storage tank. There is a convective heat transfer between the HTF and the walls of the composite-PCM enclosure. The convective heat transfer can be enhanced by increasing the flow rate through the channels. For a high flow rate, the channel wall temperatures tend to the HTF fluid temperature, and an isothermal channel wall can be assumed. The size of the storage tank depends on the intended application and can be increased by using several PCM enclosures along the channel walls.

The other enclosure's surfaces are well insulated. The enclosure could be mounted with a tilt angle δ. Thus, the gravity vector (g) acts as a body force with an inclination angle δ. The anisotropic metal foam with a porosity ε shows anisotropic permeability (K) and thermal conductivity (k) in x and y directions. Enforcing the metal foam in a direction increases the thermal conductivity but reduces the permeability. The anisotropic intensity is controlled by a parameter (K_n) and an anisotropic angle (γ). Thus, the permeability and thermal conductivity of the metal foam are introduced as

$$K = \begin{bmatrix} K_1(\cos\gamma)^2 + K_2(\sin\gamma)^2 & (K_1 - K_2)(\sin\gamma)(\cos\gamma) \\ (K_1 - K_2)(\sin\gamma)(\cos\gamma) & K_2(\cos\gamma)^2 + K_1(\sin\gamma)^2 \end{bmatrix} \quad (1)$$

$$k = \begin{bmatrix} k_1(\cos\gamma)^2 + k_2(\sin\gamma)^2 & (k_1 - k_2)(\cos\gamma)(\sin\gamma) \\ (k_1 - k_2)(\cos\gamma)(\sin\gamma) & k_1(\sin\gamma)^2 + k_2(\cos\gamma)^2 \end{bmatrix} \quad (2)$$

where $K_1 = (1 - K_n) \times K_m$, $K_2 = (1 + K_n) \times K_m$, $k_1 = (1 + K_n) \times k_m$, and $k_2 = (1 - K_n) \times k_m$. Here, K_m and k_m denote the average permeability and average thermal conductivity of the metal foam.

Initially, the enclosure is at a supper cold temperature (T_c) while the heated wall is at an isothermal hot temperature of T_h. The aim is to melt the PCM inside the enclosure as fast as possible and shorten the thermally charging process. Thus, the parameters of interest are the tilt angle (δ) and the anisotropic angle (γ). The thermophysical specifications of the copper foam and PCM are summarized in Table 1.

2.2. Governing equations

The control equations for the continuity, conservation of momentum, and heat of the PCM embedded in anisotropic metal foam are

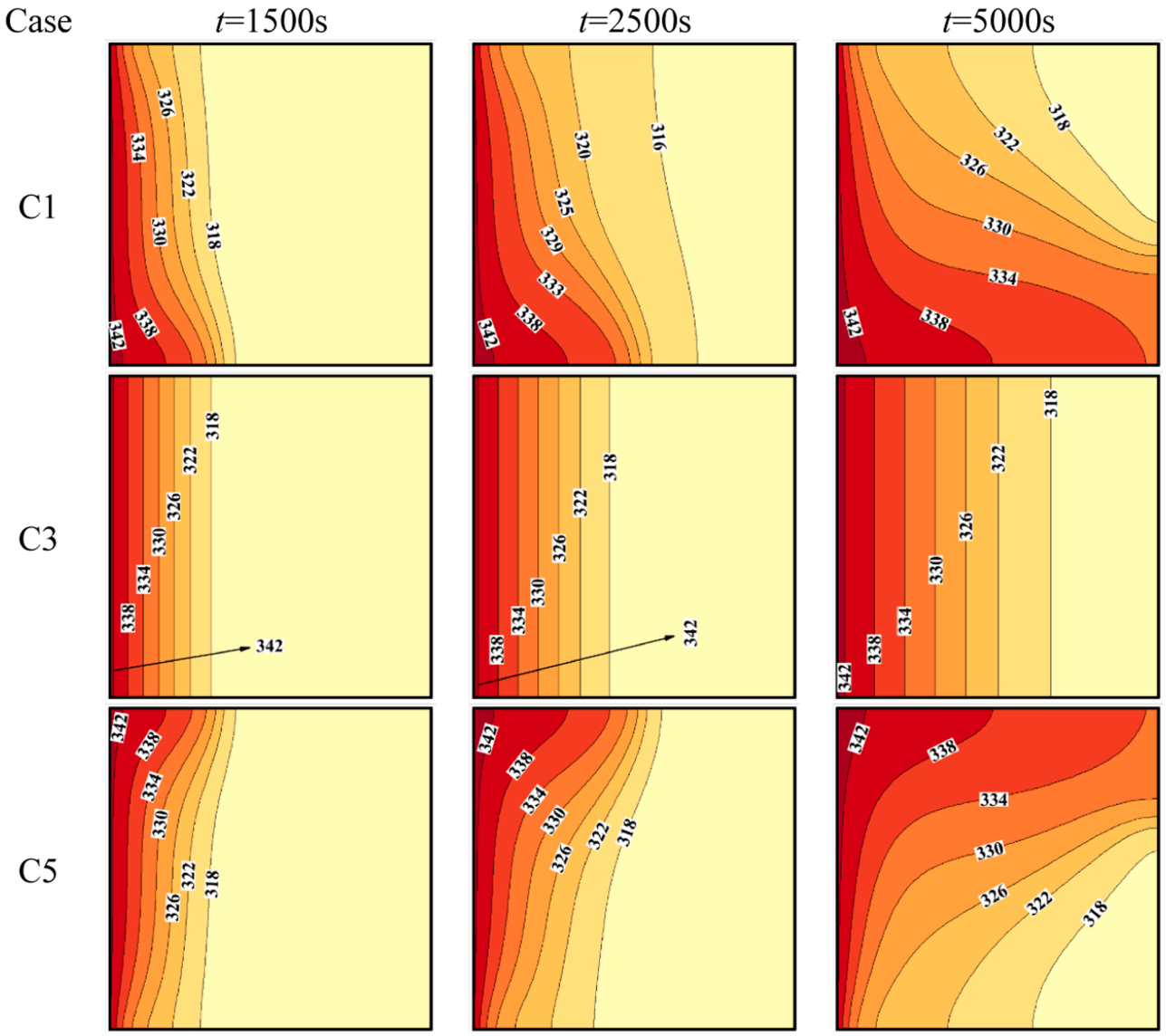

Fig. 9. Effect of inclination angle on the contour of isotherms: C1 (top row, $\delta = -45°$), C3 (middle row, $\delta = 0°$), and C5 (bottom row, $\delta = +45°$) for an anisotropic porous medium with $\gamma = -90°$. Cases C1 and C5 show similar isotherm patterns but in a mirror fashion. Case 3 shows a stratified isotherm distribution.

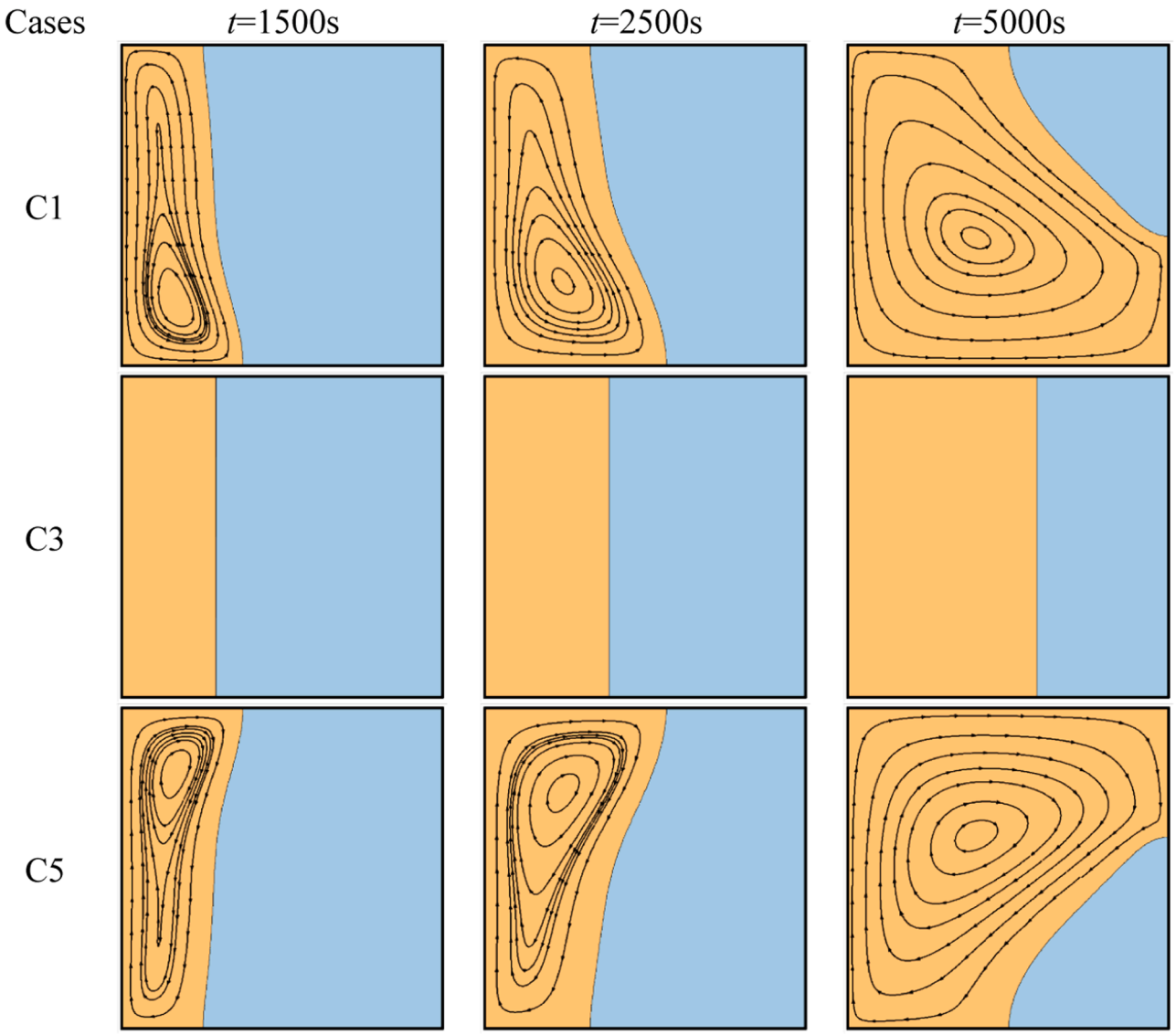

Fig. 10. Effect of inclination angle on the streamlines C1 (top row), C3 (middle row), and C5 (bottom row) for an anisotropic porous medium with $\gamma = -90^{\circ}$. Cases C1 and C15 show similar isotherm patterns but in a mirror fashion. Case 3 shows a stratified isotherm distribution.

expressed as [55]:

Continuity equation:

$$\frac{\partial u}{\partial x}+\frac{\partial v}{\partial y}=0 \tag{2}$$

Momentum equations:

$$\left(\frac{\rho_p}{\varepsilon}\right)\frac{\partial u}{\partial t}+\left(\frac{\rho_p}{\varepsilon^2}\right)\left(u\frac{\partial u}{\partial x}+v\frac{\partial u}{\partial y}\right)=-\left(\frac{\partial P}{\partial x}\right)+\left(\frac{\partial}{\partial x}\left(\frac{\mu_p}{\varepsilon}\frac{\partial u}{\partial x}\right)+\frac{\partial}{\partial y}\left(\frac{\mu_p}{\varepsilon}\frac{\partial u}{\partial y}\right)\right)$$
$$-\left(\frac{\mu_p}{\kappa(x,y)}\right)u-S(\alpha).u+\rho_p g\beta_p\cos(\delta)\left(T-T_f\right) \tag{3}$$

$$\frac{\rho_p}{\varepsilon}\frac{\partial u}{\partial t}+\frac{\rho_p}{\varepsilon^2}\left(u\frac{\partial v}{\partial x}+v\frac{\partial v}{\partial y}\right)=-\frac{\partial P}{\partial y}+\left(\frac{\partial}{\partial x}\left(\frac{\mu_p}{\varepsilon}\frac{\partial v}{\partial x}\right)+\frac{\partial}{\partial y}\left(\frac{\mu_p}{\varepsilon}\frac{\partial v}{\partial y}\right)\right)$$
$$-\frac{\mu_p}{\kappa(x,y)}v-S(\alpha).v+\rho_p g\beta_p\sin(\delta)\left(T-T_f\right) \tag{4}$$

Heat equation:

$$\left(\rho c_p\right)_{\text{eff}}\frac{\partial T}{\partial t}+\left(\rho c_p\right)_p\left(u\frac{\partial T}{\partial x}+v\frac{\partial T}{\partial y}\right)$$
$$=\frac{\partial}{\partial x}\left(k_{\text{eff,p}}(x,y)\frac{\partial T}{\partial x}\right)+\frac{\partial}{\partial y}\left(k_{\text{eff,p}}(x,y)\frac{\partial T}{\partial y}\right)-\varepsilon\rho_p L_f\frac{\partial\alpha(T)}{\partial t} \tag{5}$$

where the enthalpy-porosity approach was used for the phase transition and velocity control terms. The field variables are the velocity components (u and v), temperature (T), pressure (P), and liquid fraction (α). The material (x and y) and temporal (t) are the independent variables. The momentum equations contain a sink $S(\alpha)$, which mandates the velocities to zero in solid areas. The gravity force (g) acts with an inclination angle δ, where in the case of $\delta = 0$, the gravity is imposed horizontally (perpendicular to the heated wall). For $\delta = 90^{\circ}$, the gravity is vertically (parallel to the heated wall) and in the downward direction. The thermophysical properties are distinguished using subscripts, including the fusion property (f), effective properties (eff), phase change material (p), solid (s), and liquid (l) phases.

In the above equations, the molten PCM was considered as a laminar incompressible and Newtonian fluid. The thermophysical properties are

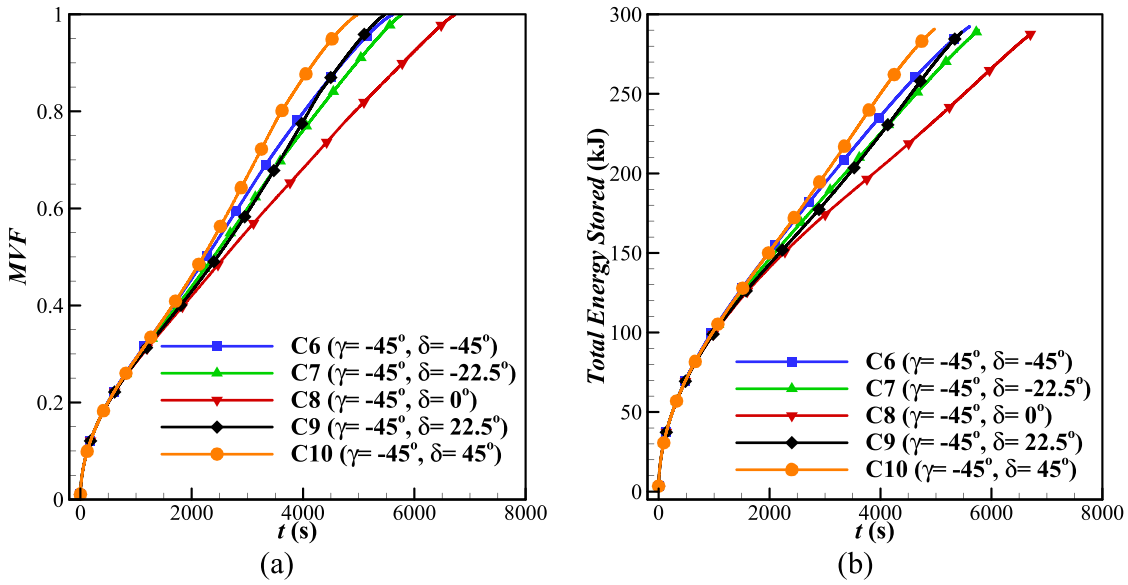

Fig. 11. Effect of inclination angle on; (a) Melting volume fraction and (b) Total energy stored in the anisotropic porous medium with $\gamma = -45^{\circ}$ (Cases C6 to C10). The case $\delta = -45^{\circ}$ provides the lowest melting time and highest heat transfer rate. The highest melting time and lowest rate of heat transfer correspond to the case $\delta = 0^{\circ}$.

constant except during the phase change. The buoyancy effects were included using the Boussinesq model. The sink term is a function of melt liquid and was computed as:

$$S(\alpha) = 10^{10}\left[1 - 2\alpha + \alpha^2\right] / \left[0.001 + \alpha^3\right] \tag{6a}$$

The physical properties are μ, L_f, ρ, β, k, and $C_{p,}$ representing the dynamic viscosity, latent heat, density, thermal expansion coefficient, thermal conductivity, and specific heat. The phase transition takes place in a small temperature interval (δT_f) around the phase change temperature (T_f). Considering a linear temperature distribution in the phase transition interval, the liquid fraction is formulated as

$$\alpha(T) = \begin{cases} 0 & T < T_f - (\Delta T_f/2) \\ \frac{1}{2} + \left(\frac{T - T_f}{\Delta T_f}\right) & T_f - (\Delta T_f/2) \langle T < T_f + (\Delta T_f/2) \\ 1 & T > T_f + (\Delta T_f/2) \end{cases} \tag{6b}$$

in which $\delta T_f = 4.7\ ^{\circ}C$. The thermal conductivity and heat capacity at the phase transition zone is a function of liquid fraction and were introduced as:

$$(\rho C_p)_p = \alpha(\rho C_p)_l + (1-\alpha)(\rho C_p)_s \tag{7a}$$

$$k_p = \alpha k_l + (1-\alpha)k_s \tag{7b}$$

Moreover, the copper foam – coconut oil effective heat capacity is computed as the average of PCM and porous phase (indicated by mf subscript) as:

$$(\rho C_p)_{\text{eff,p}} = (\rho C_p)_p + (1-\varepsilon)(\rho C_p)_{mf} \tag{8a}$$

The thermal conductivity for composite metal foam-PCM could be evaluated utilizing several literature models including [56–58]. Here, the relationship explained in [58] agrees well with the empirical data [59], and hence, it has been used here to calculate the effective thermal conductivity of the composite-PCM:

$$k_{\text{eff,p}} = \frac{1-A}{\left(\frac{\varepsilon}{k_p} + \frac{1-\varepsilon}{k_{mf}}\right)} + A\left(\varepsilon k_p + (1-\varepsilon)k_{mf}\right) \tag{8b}$$

in which the first and second terms of the equation show a serial and parallel configuration of PCM and foam, respectively. The parameter A shows a weight between the two configurations which should be considered as $A = 0.35$ based on [58]. The heat equation assumes that the temperature of PCM and metal foams at each representative element are close to each other. Besides, the density variations during the phase transition are assumed to be insignificant. The MF's permeability for a specified pore density and porosity can be evaluated utilizing the literature studies [60–63]. Considering a fixed porosity $\varepsilon = 0.95$ and a pore density of 10 PPI, the metal foam permeability was estimated as $9.654 \times 10^{-8}\ m^2$ [61–63]. The anisotropic parameter was also fixed as $K_n = 0.3$.

2.3. Boundary conditions

The enclosure surfaces are solid and impermeable; thus, the velocity components at the wall surfaces were considered zero. Besides, all surfaces were treated with zero heat flux, except the heated wall treated as an isothermal surface at $T_h = 70\ ^{\circ}C$. A uniform temperature ($T_c = 25\ ^{\circ}C$) was employed as the initial condition.

2.4. Design parameters

The total liquid fraction (MVF) and total stored energy as the design parameters were expressed as:

$$MVF = \frac{\int_A \varepsilon \alpha dA}{\int_A \varepsilon dA} \tag{9a}$$

and

$$\text{Total stored energy} = \text{sensible energy} + \text{latent energy} \tag{9b}$$

The latent energy was also computed as latent energy $= \int_A \varepsilon \alpha L_f dA$, where d$A$ is the surface element of the enclosure.

3. Numerical method, mesh sensitivity, and verification

This section concerns the numerical approach to solving mathematical equations. Then, the impact of mesh resolution is addressed on the computation's accuracy. Finally, the mathematical model and simulations are verified through comparison to literature studies.

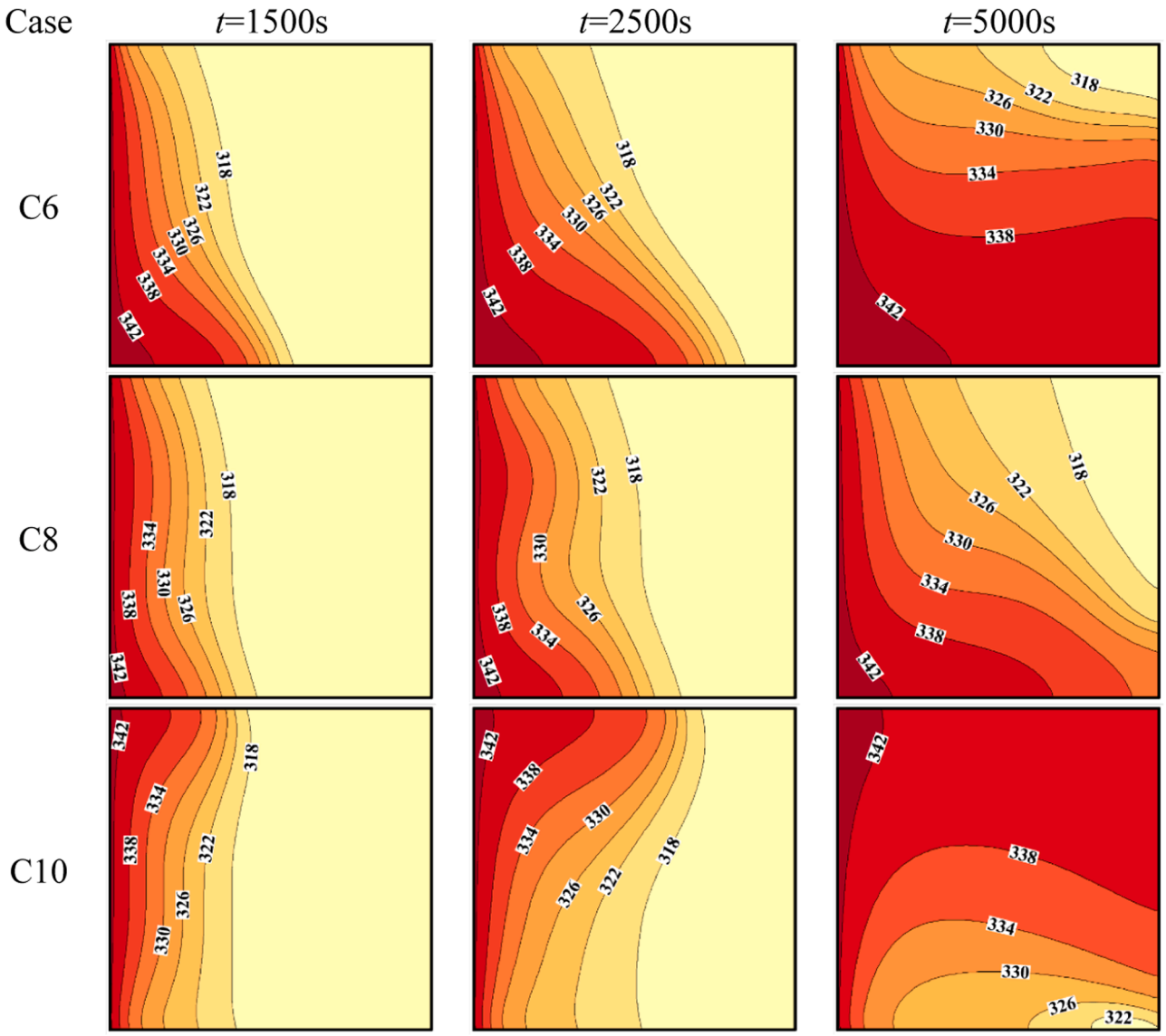

Fig. 12. Effect of inclination angle on the isotherm C6 (top row, $\delta = -45°$), C8 (middle row, $\delta = 0°$), and C10 (bottom row, $\delta = +45°$) for the anisotropic porous medium with $\gamma = -45°$. The isotherms are well dispersed for case C10.

3.1. Numerical method

The control equations and their initial and boundary conditions were solved by invoking the finite element method [64]. The equations were integrated over mesh elements using the Gauss quadrature method and the quadratic Lagrange discretization to produce a set of residual equations. The residual equations were solved in a coupled way utilizing the Newton method by employing the PARDISO parallel solver. A damped factor of 0.8 and a relative tolerance of 0.0001 was employed. The first-second order backward differential formula (BDF) was applied to adjust the time step automatically and control the solutions' accuracy with the relative tolerance [65]. The MVF was monitored as the stop condition, and the computations were terminated when MVF < 0.999. Fig. 3 illustrates a flowchart of the applied computational algorithm.

3.2. Mesh sensitivity

The influence of the mesh size on the accuracy of numerical computations was addressed by recomputing the results for various mesh resolutions. Thus, a case with $\delta = 45°$, $\gamma = 45°$, and K_n=0.3 was considered and solved for various mesh resolutions of 75 × 75, 100 × 100, 125 × 125, 150 × 150, and 175 × 175. The computed MVF during the solid-liquid phase transition is plotted in Fig. 4. As seen, the curves overlap each other, which shows the excellent accuracy of the computations. It should be noted that the time step was automatically controlled by the BDF method to keep the relative tolerance below 0.0001. It was noted that by using a mesh size of 75 × 75, the required time step sizes were reduced notably to keep the computations accurate, and thus, the overall computational time can be increased. Therefore, as a trade between the computational accuracy and computational costs, the mesh size of 100 × 100 was chosen to perform the computations in the results section.

3.3. Verification

Fahs et al. [66] investigated the natural convection follow and heat

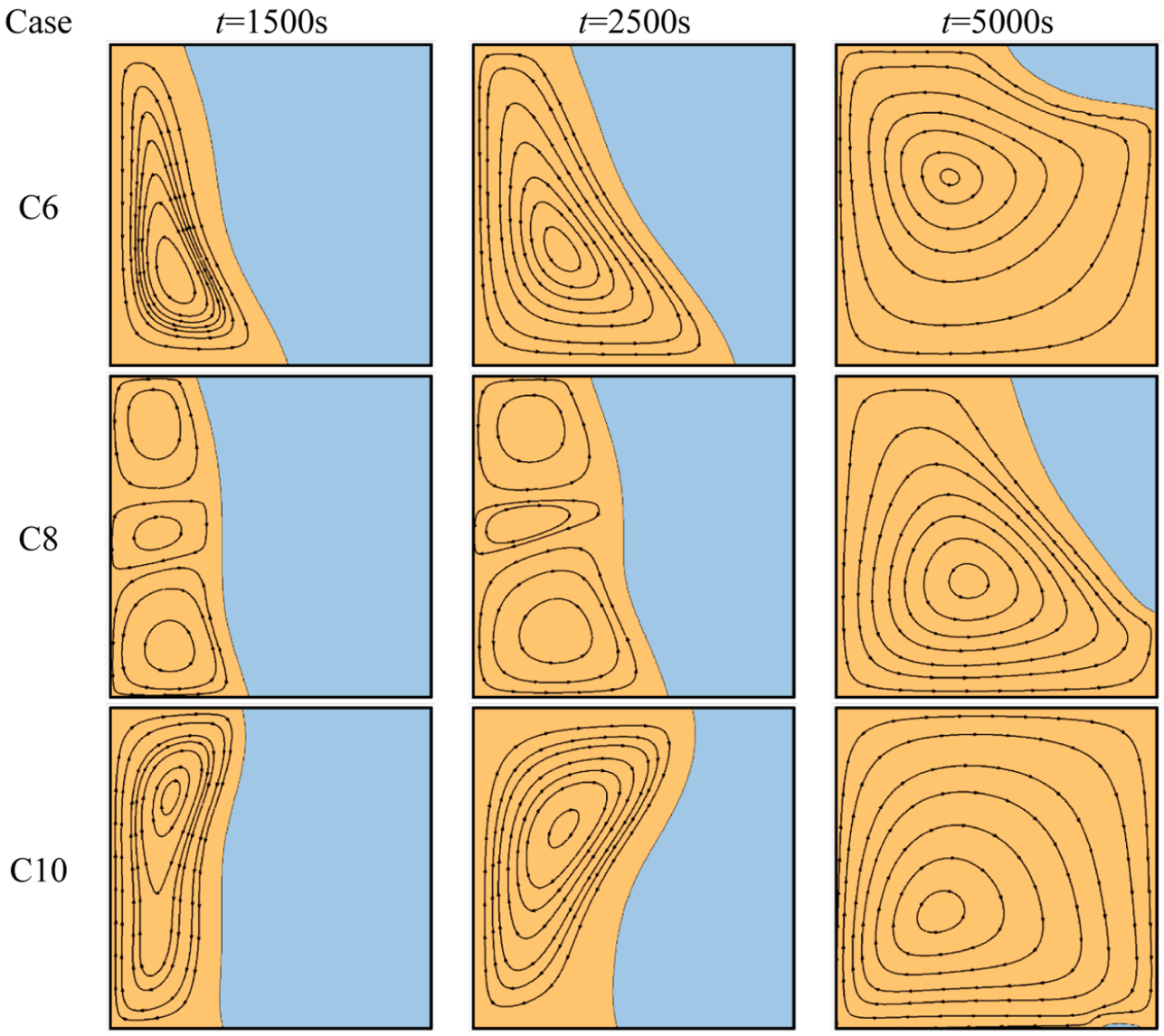

Fig. 13. Effect of inclination angle on the streamlines C6 (top row, $\delta = -45°$), C8 (middle row, $\delta = 0°$), and C10 (bottom row, $\delta = +45°$) for the anisotropic porous medium with $\gamma = -45°$. Three circulation flows can be seen for case C10 at initial times, while there is only one general circulation flow for other cases.

transfer in an anisotropic porous medium while there was a thermal conductivity gradient in x and y directions, i.e., $k(x, y)$, which was dependent on a distribution parameter ζ. For a case with $\zeta = 2.0$, the dimensionless temperatures of [66] are compared to the numerical results of the present research in Fig. 5. The results of Fig. 5 illustrate a good agreement between the current computations and the literature study.

The results of current research are compared with the measured data provided in the study of Zheng et al. [67] for melting of paraffin wax in a uniform copper foam at a 95% porosity and 5 PPI pore density. Fig. 6 illustrates the empirical and simulated data at three time-steps of 5400 s, 10,800 s, and 16,200 s. The experiments were performed in a cavity of size 100 mm × 100 mm and depth of 30 mm. The enclosure was exposed to a heat source at the side wall with a heat rate of 3.45 W, which was equal to 1150 W/m^2 for a 2D model. The PCM was initially as a super cold temperature of 14 °C with a pick melting temperature of 55.3 °C. The effective thermal conductivity and permeability were computed as 6.955 W/(m K) and 3.8614E−7 m^2, respectively. Fig. 6 demonstrates an agreement with the experimental images. Moreover, the average temperature at a vertical line with a 25 mm distance from the element (heated wall) was computed and plotted in Fig. 7. Fig. 7 depicts a comparison between the empirical [67] and numerical temperatures. This figure shows a good agreement between the simulated results of the present study and the literature experiment for melting heat transfer in metal foam.

5. Results and discussions

The current research aimed to investigate the influence of anisotropic angle (γ) and tilt angle (δ) on the charging process of an LHTES design. Here, 25 cases, according to Table 2, were simulated. The stored energy (ES), charging time, and charging power were also reported when MVF = 0.99. The charging power was computed as ES(J)/charging time(s).

Fig. 8 depicted the MVF and total stored energy for various tilted angles (δ) when the anisotropic angle was fixed at $\gamma = -90$. In this case,

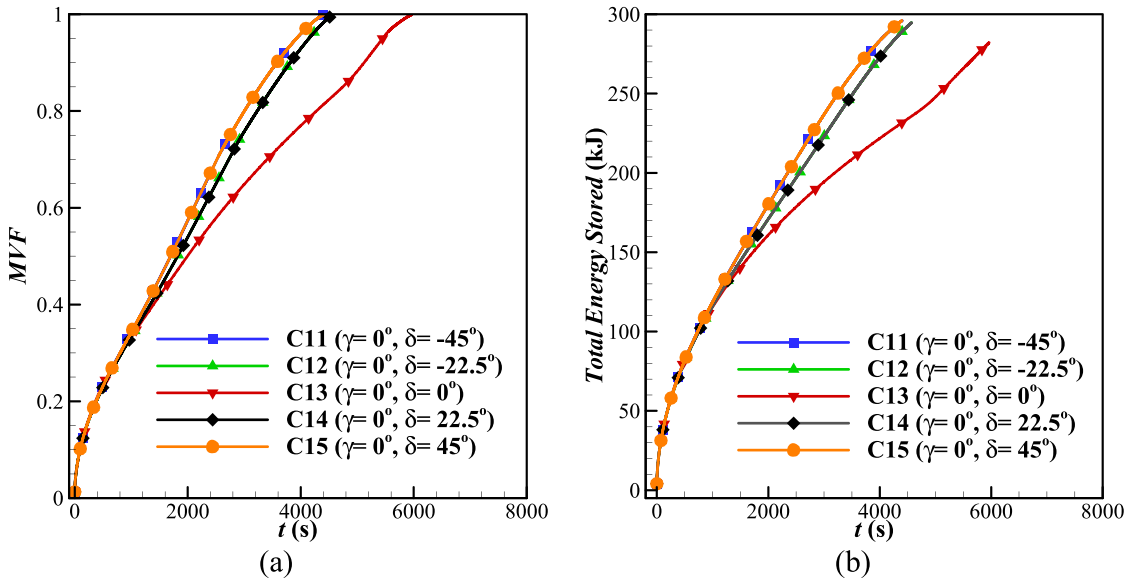

Fig. 14. Effect of inclination angle on; (a) Melting volume fraction and (b) Total energy stored in the anisotropic porous medium with $\gamma = 0^\circ$ (Cases C11 to C15). Cases $\delta = +45^\circ$ and -45° provide the shortest melting time and the highest rate of thermal energy storage. Case $\delta = 0^\circ$ corresponds to the longest melting time and lowest rate of thermal energy storage.

the thermal conductivity in the *x*-direction is reduced by 30% and increased in the y-direction by 30%. The permeability was increased and decreased by 30% in the *x*- and *y*- directions, respectively. The results are reported from the initial time with a super cold temperature until complete melting. The results show a case with zero tilt angle ($\delta = 0$ for C3) results in the slowest charging rate. The isotherms and streamlines for cases C1, C3, and C5 are depicted in Figs. 9 and 10. As seen in Fig. 9, the isotherms are distributed linearly from the heated surface toward the melting interface. Thus, the temperature distribution shows a stratified behavior. Fig. 10 also shows no streamlines. In this case, the heated surface is placed on top, the heated liquid stays next to the heated surface, and no natural convection circulation occurs. Thus, this case corresponds to the slowest heat transfer rate, and the anisotropic angle could only contribute to the conduction heat transfer mechanism by influencing the local thermal conductivity. The shortest charging time corresponds to the cases of $\delta = +45^\circ$ and $\delta = -45^\circ$. In these cases, the natural convection circulation starts from the enclosure's bottom or top regions. The energy storage curves show a trend of behavior similar to the MVF curves since the dominant mechanism of thermal energy storage is the latent heat thermal energy storage derived by the liquid fraction.

Figs. 11 and 14 depicted the influence of the tilt angle on the MVF and energy storage when the anisotropic angle was $\gamma = -90$ and $\gamma = 0^\circ$, respectively. As was observed in previous images, the case with $\delta = 0^\circ$ corresponds to the lowers heat transfer rate and energy storage rate since the isotherms are stratified. Attention to the energy curves shows they end at almost identical values of stored energy because the amount of PCM and metal foam is fixed in the enclosure regardless of tilted and anisotropic angles. Fig. 11 shows the highest heat transfer rate belongs to the case with $\delta = 45^\circ$, while Figs. 14 and 7 show both cases of $\delta = 45^\circ$ and $\delta = -45^\circ$ could equally provide the best heat transfer rate. From these images, it is evident that cases $\delta = 45^\circ$ and $\delta = -45^\circ$ are good potential cases for heat transfer improvement by enhancing the natural convection circulation flows. For cases $\gamma = 0^\circ$ (Fig. 7) and $\gamma = -90^\circ$ (Fig. 14), the anisotropic distributions are aligned with the enclosure walls. Thus, for the tilting angles $\delta = 45^\circ$ and $\delta = -45^\circ$, the anisotropic distributions would contribute to enhancing the heat transfer and flow circulation in one direction and deteriorate the heat transfer in the other perpendicular direction. Thus, the thermal behavior for both cases $\gamma = 0^\circ$ and $\gamma = -90^\circ$ are similar when $\delta = 45^\circ$ and $\delta = -45^\circ$. However, case $\gamma = 45^\circ$ (Fig. 11) is different. In this case, there is a 45° anisotropic local distribution, and tilting the enclosure by 45° would improve the natural convection circulation and benefit from the local enhancement of heat transfer and the conduction heat transfer. Figs. 12, 13, 15, and 16 show the isotherms and streamlines for two cases of $\gamma = 0^\circ$ and $\gamma = -90^\circ$. Figs. 15 and 16 confirm similar melting front, temperature distribution, and streamlines for cases $\delta = 45^\circ$(C15) and $\delta = -45^\circ$ (C11), with the only difference that the convection is downward for C11 and upward for C15. As discussed, the stratified case (C13) streamlines were not plotted. Attention to the shape of the melting front for case C15 shows a sharp convection heat transfer at the top region (compared to Figs. 8 and 9) due to the improved thermal conductivity in the *x*-direction and improved permeability in the *y*-direction. The improved *x*-thermal conductivity better diffuses the heat deep into the enclosure, while improved *y*-permeability allows a better flow circulation.

The streamlines were also plotted for case C8 since the anisotropic behavior of the metal foam breached the perfect stratification, and a slight convection flow was observed. Besides, attention to the isotherm and streamlines of Figs. 12 and 13 show the melting front is advancing from the bottom for C6, which is typical due to the natural convection effects and gravity direction. However, case C10 shows almost a uniform melting front with a good circulation flow. This is due to isotherms also showing good curvatures, which indicates strong temperature gradients. In this case, the alignment of the anisotropic angle contributes to the conduction heat transfer mechanism and convective heat transfer mechanism. It adequately advances the melting front from top to bottom. It can be seen that the whole enclosure is in liquid states at the last time snap of 5000 s.

Fig. 17 depicts the results of Table 2 in a graphical format. This figure illustrates the impact of tilt and anisotropic angles on the charging time (17a) and power (17b). A general view of the curves shows the charging power follows the charging time trend but in a reverse direction.

It is clear that an anisotropic angle can significantly change the melting time and power. The maximum power can be achieved for γ at tilt angles of -45° or $+45^\circ$. The minimum power can be seen for $\gamma = -90^\circ$ and zero tilt angle. In this case, there is no natural convection (stratified temperature distribution), and the thermal conductivity is minimal perpendicular to the heated surface. Thus, the thermal

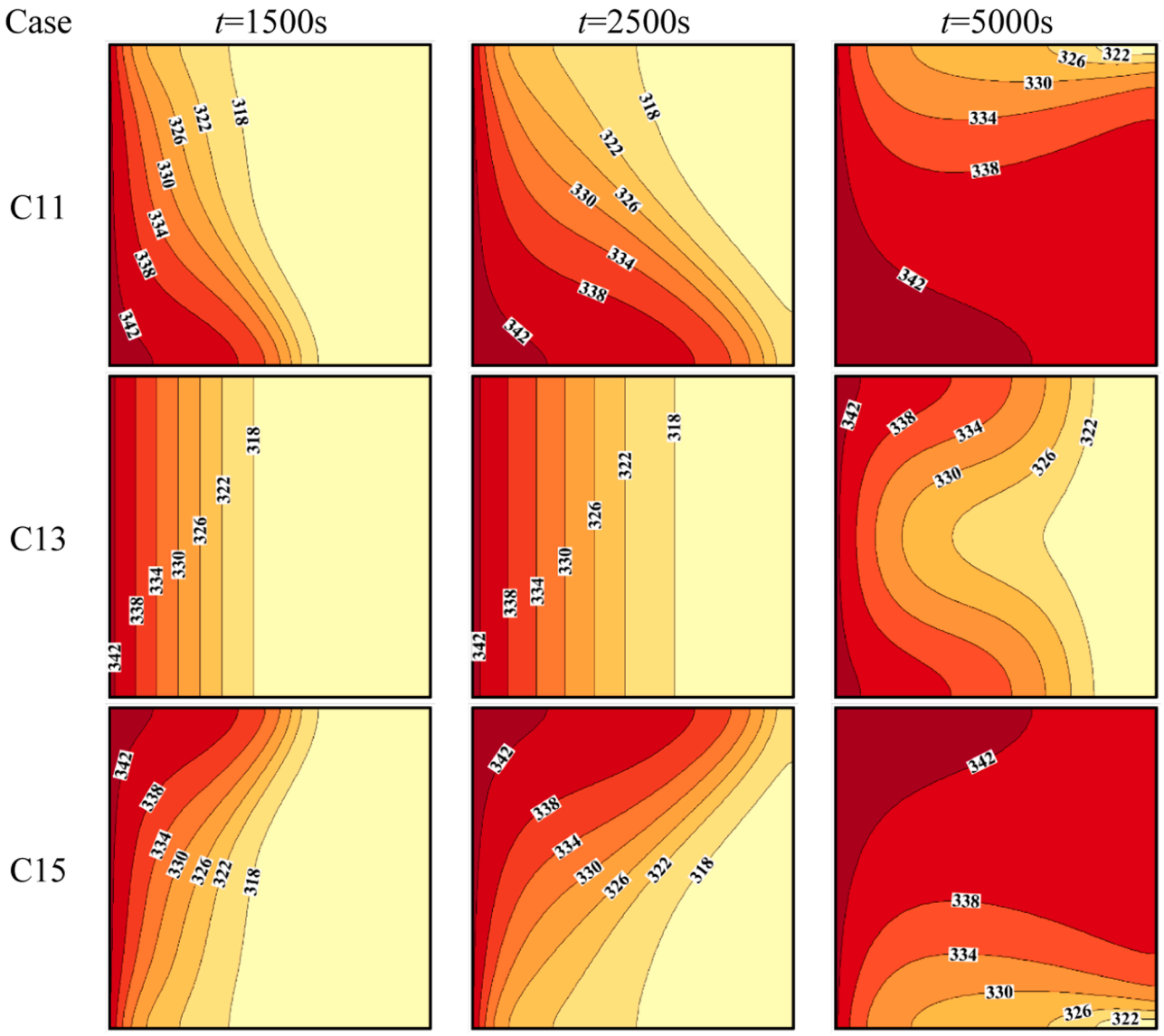

Fig. 15. Effect of inclination angle on the isotherm C11 (top row, $\delta = -45°$), C13 (middle row, $\delta = 0°$), and C15 (bottom row, $\delta = +45°$) for the anisotropic porous medium with $\gamma = 0°$. Cases C11 and C15 show similar isotherm patterns but in a mirror fashion. Case 13 shows a stratified isotherm distribution.

conductivity distribution significantly weakens the only mechanism of heat transfer, which is the conduction heat transfer mechanism. The difference between the maximum power (C11 and C15) with 68.4 and the minimum power (C3) with 27.3 W is 41.1 W.

The results were also computed for five inclination angles of $-45°$, $-22.5°$, $0°$, $22.5°$, and $45°$ when $K_n = 0$ (isotropic MF). The full charging time was computed as 83min ($-45°$), 88 min ($-22.5°$), 116 min ($0°$), 88 min ($22.5°$), and 83 min ($45°$). As seen, there is asymmetry between the results around $0°$, which is due to the presence of isotropic MF. A comparison of these data to the results of Fig. 17(a) for $K_n = 0.3$ and $\gamma = 0°$ shows the charging time was decreased by (83 min-71 min)/83 min = 15% for $\delta = -45°$, (88 min-74 min)/83 min=16% for $\delta = -22.5°$, and (116 min-97 min)/97 min = 20% for $\delta = -22.5°$. Almost similar results can be found for inclination angles of $\delta = +22.5°$ and $\delta = +45°$. However, using not well-designed anisotropic angle $\gamma = -90$ could increase the melting time by 28%, 32%, and 45%, respectively for inclination angles of $\delta = -45°$, $\delta = -22.5°$, and $\delta = 0°$ compared to a similar isotropic MF. Thus, proper design and selection of anisotropic angle is a crucial task.

6. Conclusions

The phase change flow and heat transfer in an anisotropic metal foam were modeled using an enthalpy-porosity approach. The anisotropic properties, including the thermal conductivity and permeability, were defined using 2D tensors and controlled by an anisotropic parameter and angle. The finite element method with automatic time step control was applied to solve the governing equations. The weight of the metal foam was constant, and the anisotropic distribution changed the properties in perpendicular directions. The influence of a tilt angle was also addressed on the phase transition behavior in the presence of anisotropic properties. The isotherms and streamlines were also reported to reveal the impact of anisotropic and tilt angles on the phase transition process and thermal energy storage.

- The result showed an anisotropic angle could significantly influence the phase transition time and charging power. Placing the metal foam with a zero anisotropic angle results in the best heat transfer rate and shortest charging time when the tilt angle is $+45°$ or $-45°$. A

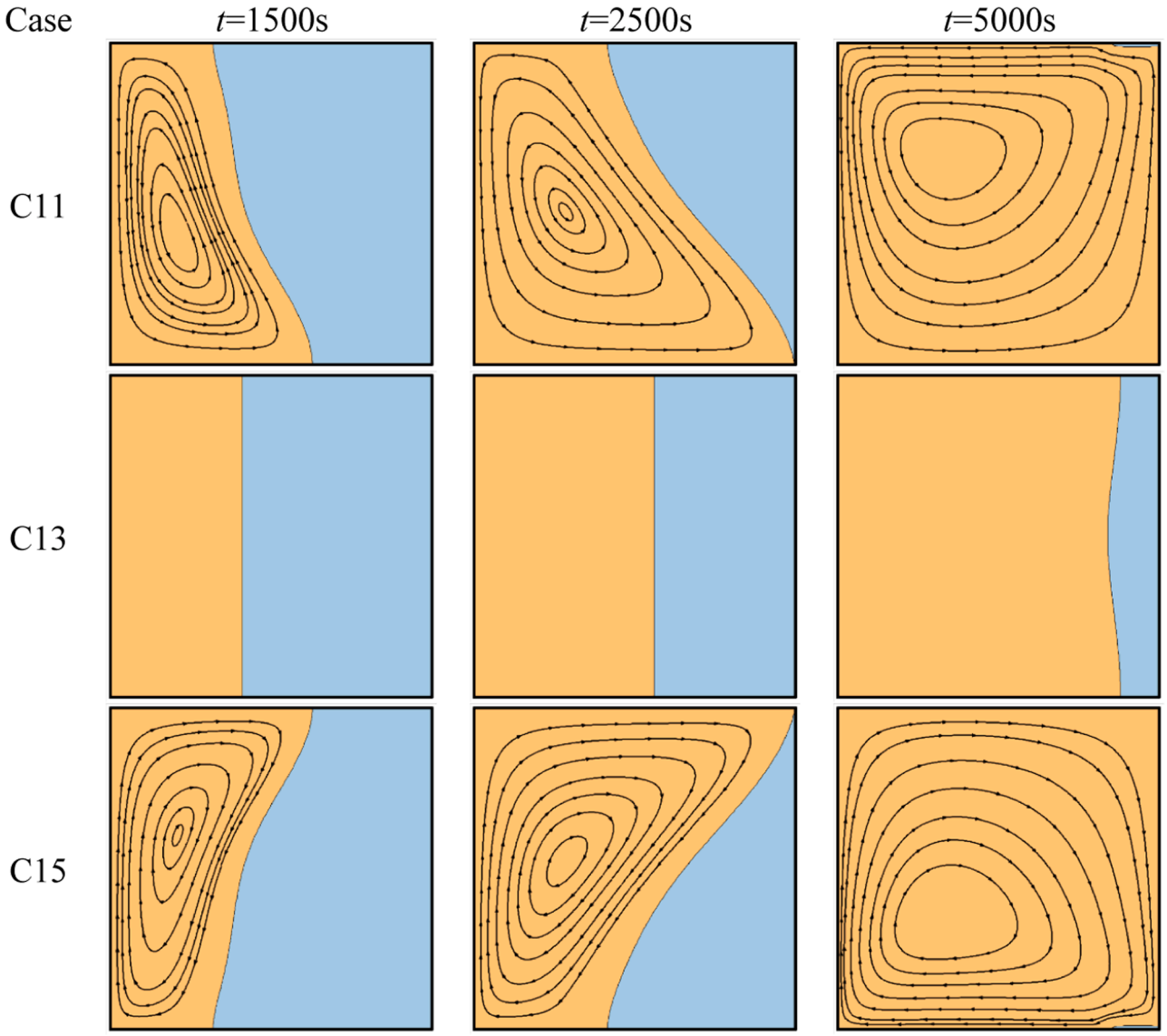

Fig. 16. Effect of inclination angle on the streamlines C11 (top row, $\delta = -45^\circ$), C13 (middle row, $\delta = 0^\circ$), and C15 (bottom row, $\delta = +45^\circ$) for the anisotropic porous medium with $\gamma = 0^\circ$. Cases C11 and C15 show similar streamline patterns but in a mirror fashion. Case 13 shows no significant circulation due to the stratified nature of isotherms.

zero anisotropic angle increases the thermal conductivity along the *x*-direction and the permeability along the *y*-direction. Thus, the anisotropic alignment facilitates the liquid motion parallel to the heated wall and improves thermal diffusion perpendicular to the heated surface. As a result, the heat could be transferred into the enclosure by the conduction mechanism and then carried out in a perpendicular direction more easily for an anisotropic metal foam. In contrast, a not well alignment of anisotropic properties could deteriorate the conduction heat transfer in an essential direction and decreases the overall heat transfer rate. Thus, selecting the anisotropic angle is a crucial parameter in designing an LHTES unit. An anisotropic metal foam with an anisotropic angle $\gamma = 0$ could save the thermal charging time about 15% when $\delta = -45^\circ$ and −20% when $\delta = 0^\circ$ compared to a uniform isotropic MF. However, using an anisotropic angle $\gamma = -90^\circ$ could increase the charging time by 28% ($\delta = -45^\circ$), 32% ($\delta = -22.5^\circ$), and 45% ($\delta = -0^\circ$).

- A tilt angle can also influence the heat transfer rate. Mounting the units with a tilted angle of $+45^\circ$ or -45° results in the maximum charging power. A tilted angle of 0° results in stratified temperature distribution, significantly reduces the heat transfer rate, and increases the charging time.
- A combination of $+45^\circ$ or -45° tilt angle and 0° anisotropic angle leads to the maximum charging power. It should be noted that variation of the tilt and the anisotropic angles does not change the amount (weight) of the metal foam and the LHTES unit. Thus, heat transfer improvement could be achieved with no weight increase or capacity reduction penalty.

The results of the present study show that using anisotropic metal foam can considerably save the melting time and improve the thermal energy storage rate. The future works can consider using anisotropic metal foams in fin MF shapes or anisotropic MF layers in LHTES designs. Moreover, the solidification time is another important aspect of LHTES systems which can be investigated for anisotropic MFs in future studies.

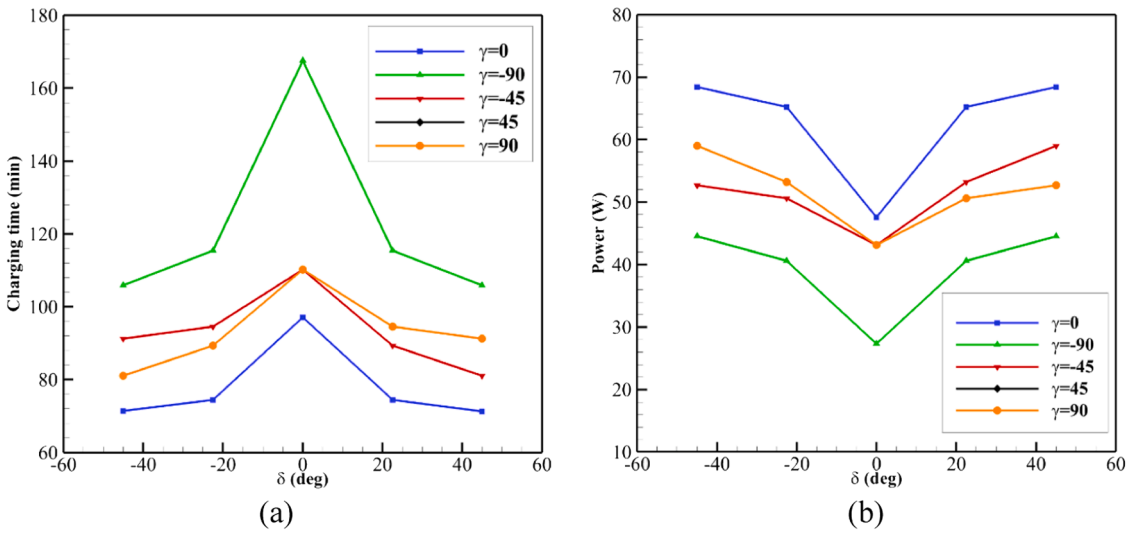

Fig. 17. Effect of inclination angle on; (a) melting time and (b) energy sortation power for various values of the anisotropic angle (γ). Case $\gamma = 0°$ generally provides the highest charging power and shortest charging time. The maximum charging power can be observed at $\delta = +45°$ and $\delta = -45°$.

CRediT authorship contribution statement

Mehdi Ghalambaz: Conceptualization, Methodology, Software, Validation, Formal analysis, Data curation. **Mutabe Aljaghtham:** Visualization, Writing – original draft, Investigation, Formal analysis, Data curation. **Ali J. Chamkha:** Visualization, Writing – original draft, Investigation, Formal analysis, Data curation. **Abdelkader Abdullah:** Methodology, Software, Formal analysis, Data curation. **Abdullah Alshehri:** Methodology, Software, Formal analysis, Data curation. **Mohammad Ghalambaz:** Investigation, Writing – review & editing, Supervision.

Declaration of Competing Interest

Authors declare that they have no conflict of interest.

Data availability

No data was used for the research described in the article.

Acknowledgment

The authors extend their appreciation to the Deputyship for Research & Innovation, Ministry of Education in Saudi Arabia for funding this research work through the project number (IF-PSAU-2021/01/18928).

References

[1] Alva G, Lin Y, Fang G. An overview of thermal energy storage systems. Energy 2018;144:341–78.
[2] Huang Y, Pang Z, Kong Y, Watanabe N. Assessment of the high-temperature aquifer thermal energy storage (HT-ATES) potential in naturally fractured geothermal reservoirs with a stochastic discrete fracture network model. J Hydrol 2021;603.
[3] Cheng P, Chen X, Gao H, Zhang X, Tang Z, Li A, Wang G. Different dimensional nanoadditives for thermal conductivity enhancement of phase change materials: fundamentals and applications. Nano Energy 2021;85.
[4] Motahar S, Khodabandeh R. Experimental study on the melting and solidification of a phase change material enhanced by heat pipe. Int Commun Heat Mass Transf 2016;73:1–6.
[5] Guo J, Liu Z, Yang B, Yang X, Yan J. Melting assessment on the angled fin design for a novel latent heat thermal energy storage tube. Renew Energy 2022;183:406–22.
[6] Guo J, Wang X, Yang B, Yang X, Li MJ. Thermal assessment on solid-liquid energy storage tube packed with non-uniform angled fins. Sol Energy Mater Sol Cells 2022;236:111526.
[7] Yang X, Wang X, Liu Z, Luo X, Yan J. Effect of fin number on the melting phase change in a horizontal finned shell-and-tube thermal energy storage unit. Sol Energy Mater Sol Cells 2022;236:111527.
[8] Yu XK, Tao YB, He Y, Lv ZC. Preparation and performance characterization of metal foam/paraffin/single-walled carbon nanotube composite phase change material. Int J Heat Mass Transf 2022;191.
[9] Li X, Li H, Kong X, Yang H. Characterization and experimental investigation of composite phase change materials based on aluminum nitride/expanded graphite. J Energy Storage 2021;35.
[10] Najim FT, Bahlekeh A, Mohammed HI, Dulaimi A, Abed AM, Ibrahem RK, Al-Qrimli FA, Mahmoud MZ, Awrejcewicz J, Pawłowski W. Evaluation of melting mechanism and natural convection effect in a triplex tube heat storage system with a novel fin arrangement. Sustainability 2022;14:10982.
[11] Tiji ME, Al-Azzawi WK, Mohammed HI, Dulaimi A, Rashid FL, Mahdi JM, et al. Thermal management of the melting process in a latent heat triplex tube storage system using different configurations of frustum tubes. J. Nanomater. 2022;2022:14.
[12] Mahdi JM, Mohammed HI, Talebizadehsardari P. A new approach for employing multiple PCMs in the passive thermal management of photovoltaic modules. Sol Energy 2021;222:160–74.
[13] Eisapour AH, Eisapour M, Mohammed HI, Shafaghat A, Ghalambaz M, Talebizadehsardari P. Optimum design of a double elliptical latent heat energy storage system during the melting process. J Energy Storage 2021;44:103384.
[14] S.K. Razack, Thermal management system and device, in, KHATEEB RAZACK, SIDDIQUE ALI, European Patent Office, 2020.
[15] Ferfera RS, Madani B, Serhane R. Investigation of heat transfer improvement at idealized microcellular scale for metal foam incorporated with paraffin. Int J Therm Sci 2020;156.
[16] Prieto C, Lopez-Roman A, Martínez N, Morera JM, Cabeza LF. Improvement of phase change materials (PCM) used for solar process heat applications. Molecules 2021;26.
[17] Li ZB, Li XY, Zheng YX. Biaxial mechanical behavior of closed-cell aluminum foam under combined shear—compression loading. Trans Nonferrous Met Soc China 2020;30:41–50.
[18] Baby R, Balaji C. Experimental investigations on thermal performance enhancement and effect of orientation on porous matrix filled PCM based heat sink. Int Commun Heat Mass Transf 2013;46:27–30.
[19] Yang X, Wei P, Wang X, He YL. Gradient design of pore parameters on the melting process in a thermal energy storage unit filled with open-cell metal foam. Appl Energy 2020;268.
[20] Zhu F, Zhang C, Gong X. Numerical analysis on the energy storage efficiency of phase change material embedded in finned metal foam with graded porosity. Appl Therm Eng 2017;123:256–65.
[21] Mahdi JM, Nsofor EC. Multiple-segment metal foam application in the shell-and-tube PCM thermal energy storage system. J Energy Storage 2018;20:529–41.
[22] Xu Y, Li MJ, Zheng ZJ, Xue XD. Melting performance enhancement of phase change material by a limited amount of metal foam: configurational optimization and economic assessment. Appl Energy 2018;212:868–80.
[23] Joshi V, Rathod MK. Thermal performance augmentation of metal foam infused phase change material using a partial filling strategy: an evaluation for fill height ratio and porosity. Appl Energy 2019;253.
[24] Guo J, Du Z, Liu G, Yang X, Li M-J. Compression effect of metal foam on melting phase change in a shell-and-tube unit. Appl Therm Eng 2022;206:118124.
[25] Liu G, Xiao T, Guo J, Wei P, Yang X, Hooman K. Melting and solidification of phase change materials in metal foam filled thermal energy storage tank: evaluation on gradient in pore structure. Appl Therm Eng 2022;212:118564.

[26] Vijay D, Goetze P, Wulf R, Gross U. Homogenized and pore-scale analyses of forced convection through open cell foams. Int J Heat Mass Transf 2018;123:787–804.
[27] Yang J, Yang L, Xu C, Du X. Numerical analysis on thermal behavior of solid–liquid phase change within copper foam with varying porosity. Int J Heat Mass Transf 2015;84:1008–18.
[28] Huang X, Sun C, Chen Z, Han Y. Experimental and numerical studies on melting process of phase change materials (PCMs) embedded in open-cells metal foams. Int J Therm Sci 2021;170.
[29] Bamdezh MA, Molaeimanesh GR, Zanganeh S. Role of foam anisotropy used in the phase-change composite material for the hybrid thermal management system of lithium-ion battery. J Energy Storage 2020;32.
[30] Yu P, Wang Y, Ji R, Wang H, Bai J. Pore-scale numerical study of flow characteristics in anisotropic metal foam with actual skeleton structure. Int Commun Heat Mass Transf 2021;126.
[31] Ren Q, Wang Z, Lai T, Zhang JF, Qu ZG. Conjugate heat transfer in anisotropic woven metal fiber-phase change material composite. Appl Therm Eng 2021;189.
[32] Opolot M, Zhao C, Liu M, Mancin S, Bruno F, Hooman K. Influence of cascaded graphite foams on thermal performance of high temperature phase change material storage systems. Appl Therm Eng 2020;180.
[33] Zhao C, Opolot M, Liu M, Bruno F, Mancin S, Hooman K. Phase change behaviour study of PCM tanks partially filled with graphite foam. Appl Therm Eng 2021;196.
[34] Yang X, Guo Z, Liu Y, Jin L, He YL. Effect of inclination on the thermal response of composite phase change materials for thermal energy storage. Appl Energy 2019; 238:22–33.
[35] Kamkari B, Shokouhmand H, Bruno F. Experimental investigation of the effect of inclination angle on convection-driven melting of phase change material in a rectangular enclosure. Int J Heat Mass Transf 2014;72:186–200.
[36] Dhaidan NS, Khodadadi JM. Melting and convection of phase change materials in different shape containers: a review. Renew Sustain Energy Rev 2015;43:449–77.
[37] Vogel J, Felbinger J, Johnson M. Natural convection in high temperature flat plate latent heat thermal energy storage systems. Appl Energy 2016;184:184–96.
[38] Iasiello M, Bianco N, Chiu WKS, Naso V. Thermal conduction in open-cell metal foams: anisotropy and representative volume element. Int J Therm Sci 2019;137: 399–409.
[39] Iasiello M, Bianco N, Chiu WKS, Naso V. Anisotropic convective heat transfer in open-cell metal foams: Assessment and correlations. Int J Heat Mass Transf 2020; 154.
[40] Iasiello M, Mameli M, Filippeschi S, Bianco N. Metal foam/PCM melting evolution analysis: orientation and morphology effects. Appl Therm Eng 2021;187.
[41] Xie J, Lee HM, Xiang J. Numerical study of thermally optimized metal structures in a phase change material (PCM) enclosure. Appl Therm Eng 2019;148:825–37.
[42] Xie J, Luo W, Zhang W, Wu Z, Lee HM. Investigations of optimized fin structures in a compact thermal energy storage panel. IOP Conf Ser 2020;467.
[43] Yazici MY, Avci M, Aydin O. Combined effects of inclination angle and fin number on thermal performance of a PCM-based heat sink. Appl Therm Eng 2019;159.
[44] Kamkari B, Groulx D. Experimental investigation of melting behaviour of phase change material in finned rectangular enclosures under different inclination angles. Exp Therm Fluid Sci 2018;97:94–108.
[45] Karami R, Kamkari B. Investigation of the effect of inclination angle on the melting enhancement of phase change material in finned latent heat thermal storage units. Appl Therm Eng 2019;146:45–60.
[46] Samimi Behbahan A, Noghrehabadi A, Wong CP, Pop I, Behbahani-Nejad M. Investigation of enclosure aspect ratio effects on melting heat transfer characteristics of metal foam/phase change material composites. Int J Numer Methods Heat Fluid Flow 2019;29:2994–3011.
[47] Meng X, Liu S, Zou J, Liu F, Wang J. Inclination angles on the thermal behavior of phase-change material (PCM) in a cavity filled with copper foam partly. Case Stud Therm Eng 2021;25.
[48] Bouzennada T, Mechighel F, Ismail T, Kolsi L, Ghachem K. Heat transfer and fluid flow in a PCM-filled enclosure: effect of inclination angle and mid-separation fin. Int Commun Heat Mass Transf 2021;124.
[49] Tian W, Dang S, Liu G, Guo Z, Yang X. Thermal transport in phase change materials embedded in metal foam: evaluation on inclination configuration. J Energy Storage 2021;33.
[50] Kasper L, Pernsteiner D, Koller M, Schirrer A, Jakubek S, Hofmann R. Numerical studies on the influence of natural convection under inclination on optimal aluminium proportions and fin spacings in a rectangular aluminium finned latent-heat thermal energy storage. Appl Therm Eng 2021;190.
[51] Li H, Hu C, He Y, Tang D, Wang K, Hu X. Influence of model inclination on the melting behavior of graded metal foam composite phase change material: a pore-scale study. J Energy Storage 2021;44.
[52] Huang S, Lu J, Li Y. Numerical study on the influence of inclination angle on the melting behaviour of metal foam-PCM latent heat storage units. Energy 2022;239.
[53] Al-Jethelah M, Ebadi S, Venkateshwar K, Tasnim SH, Mahmud S, Dutta A. Charging nanoparticle enhanced bio-based PCM in open cell metallic foams: an experimental investigation. Appl Therm Eng 2019;148:1029–42.
[54] Choi SK, Kim SO, Lee TH, Hahn D. Computation of the natural convection of nanofluid in a square cavity with homogeneous and nonhomogeneous models. Numer Heat Transf Part A 2014;65:287–301.
[55] Zadeh SMH, Mehryan S, Ghalambaz M, Ghodrat M, Young J, Chamkha A. Hybrid thermal performance enhancement of a circular latent heat storage system by utilizing partially filled copper foam and Cu/GO nano-additives. Energy 2020;213: 118761.
[56] Yang XH, Bai JX, Yan HB, Kuang JJ, Lu TJ, Kim T. An analytical unit cell model for the effective thermal conductivity of high porosity open-cell metal foams. Transp Porous Media 2014;102:403–26.
[57] Yang X, Kuang J, Lu T, Han F, Kim T. A simplistic analytical unit cell based model for the effective thermal conductivity of high porosity open-cell metal foams. J Phys D 2013;46:255302.
[58] Bhattacharya A, Calmidi VV, Mahajan RL. Thermophysical properties of high porosity metal foams. Int J Heat Mass Transf 2002;45:1017–31.
[59] Xiao X, Zhang P, Li M. Preparation and thermal characterization of paraffin/metal foam composite phase change material. Appl Energy 2013;112:1357–66.
[60] Yang X, Lu TJ, Kim T. An analytical model for permeability of isotropic porous media. Phys Lett A 2014;378:2308–11.
[61] Nield DA, Bejan A. Convection in porous media. Springer; 2006.
[62] Mahdi JM, Nsofor EC. Melting enhancement in triplex-tube latent heat energy storage system using nanoparticles-metal foam combination. Appl Energy 2017; 191:22–34.
[63] Sardari PT, Mohammed HI, Giddings D, walker GS, Gillott M, Grant D. Numerical study of a multiple-segment metal foam-PCM latent heat storage unit: effect of porosity, pore density and location of heat source. Energy 2019;189.
[64] Zienkiewicz OC, Taylor RL, Nithiarasu P. The finite element method for fluid dynamics. 7th ed. Oxford: Butterworth-Heinemann; 2014.
[65] Söderlind G, Wang L. Adaptive time-stepping and computational stability. J Comput Appl Math 2006;185:225–43.
[66] Fahs M, Younes A, Makradi A. A reference benchmark solution for free convection in a square cavity filled with a heterogeneous porous medium. Numer Heat Transf, Part B 2015;67:437–62.
[67] Zheng H, Wang C, Liu Q, Tian Z, Fan X. Thermal performance of copper foam/ paraffin composite phase change material. Energy Convers Manag 2018;157: 372–81.